Electronic Supplementary Material (ESI) for Journal of Materials Chemistry

Supporting Information

The structural evolution and diffusion during the chemical transformation from cobalt to cobalt phosphide nanoparticles

*Don-Hyung Ha, Liane M. Moreau, Clive R. Bealing, Haitao Zhang, Richard G. Hennig, and Richard D. Robinson**

Department of Materials Science and Engineering, Cornell University, Ithaca, NY 14853

* To whom correspondence should be addressed. E-mail: rdr82@cornell.edu.

Summary

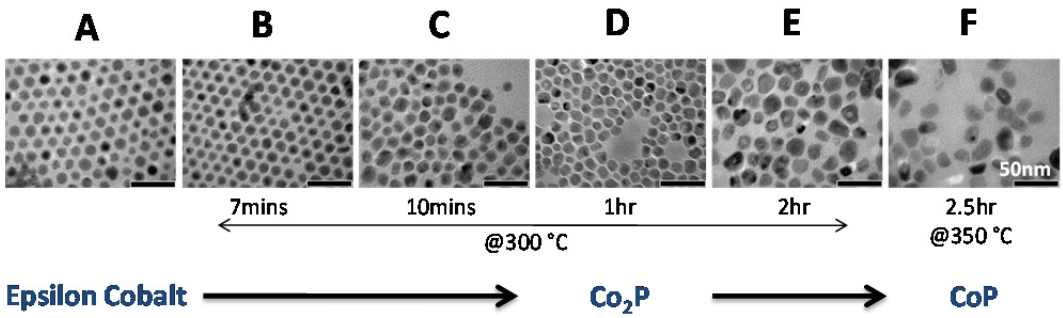

	A	B	C	D	E	F
Size(nm)	11.9	12.4	13.1	12.8	15.7	16.2
Std Dev (nm)	0.98 (8%)	1.2 (10%)	1.6 (12%)	2.0 (16%)	3.1 (20%)	3.3 (20%)
XRD	ε-Co	Mostly ε-Co	Mostly Co_2P	Co_2P	Co_2P + CoP	CoP
EXAFS Co-P Degeneracy	Co-O 0.98(Bulk:6)	3.4	4.4	4.7 (Bulk:4.5)	5.9	5.5 (Bulk:6)
EXAFS Co-Co Degeneracy	11.1 (Bulk:12)	10.2	10.2	9.9 (Bulk:9)	8.1	7.5 (Bulk:6)
Morphology	Solid Sphere	Core-shell		Hollow (70%, 3.5nm)	Hollow (30%, 5.5nm)	Hollow (20%, 4nm)

Fig. S1 Summary of reaction conditions for NP samples with corresponding TEM images directly above, and summary of XRD, EXAFS and other characterizations below.

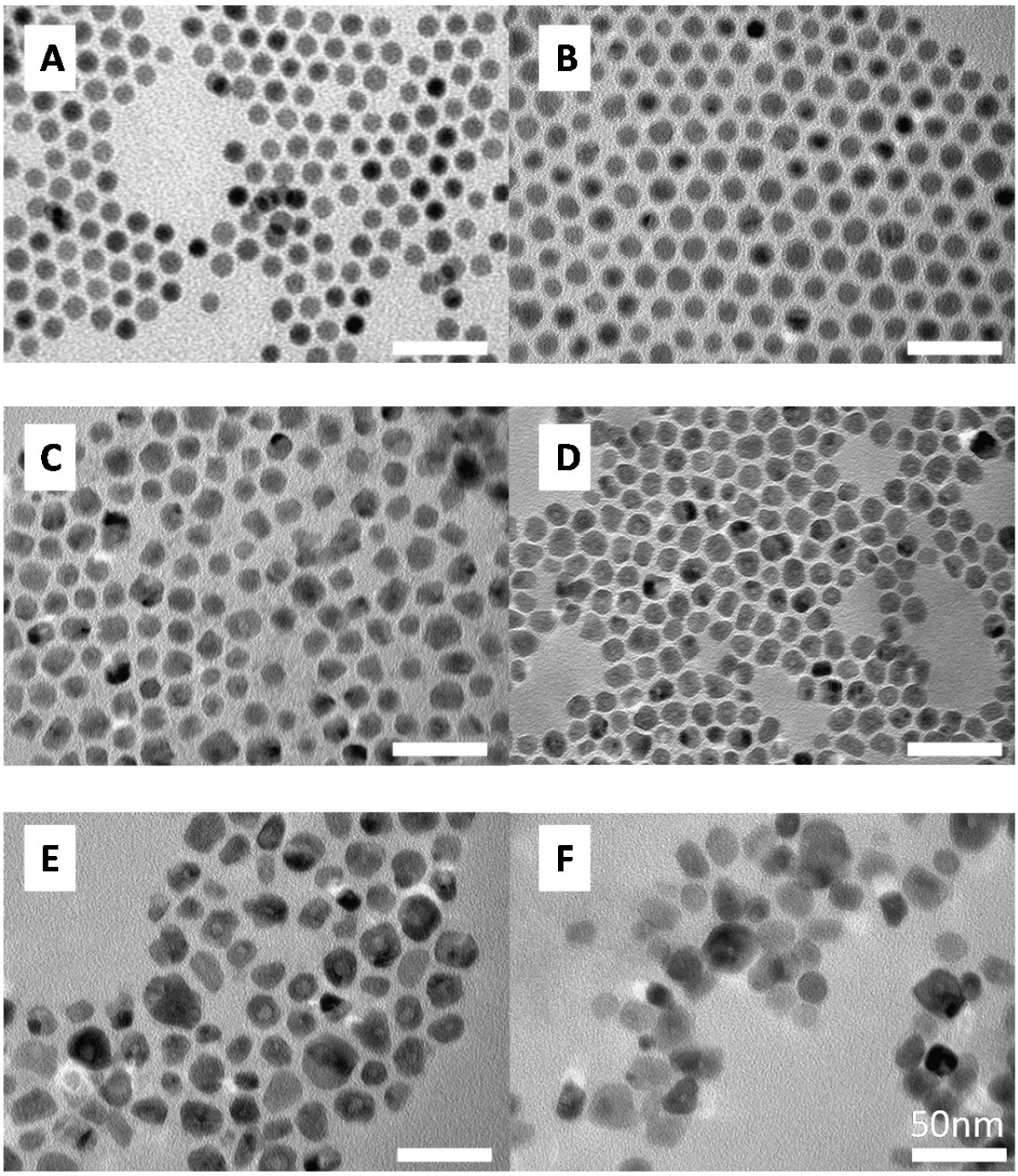

Fig. S2 Low magnification TEM images of sample **A-F**

Structure details

1) ε-Co

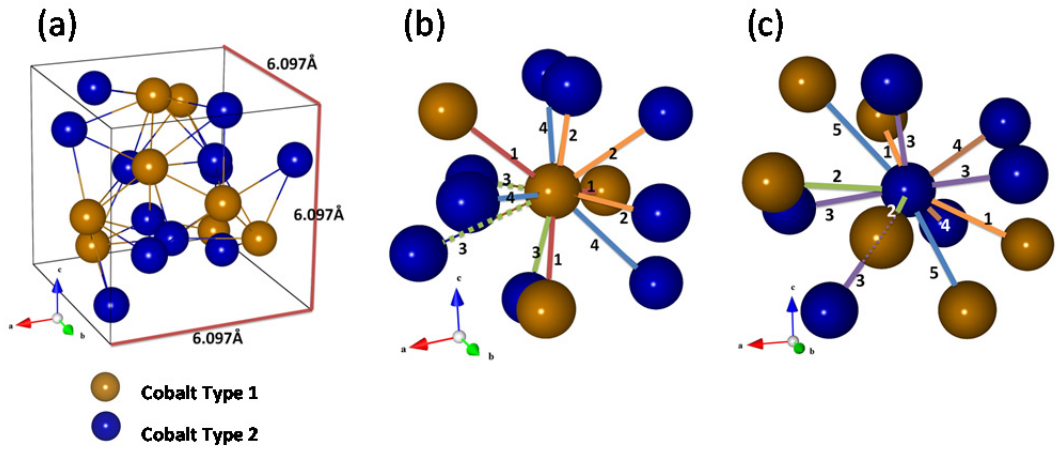

Fig. S3 (a) A schematic representation of the ε-Co crystal structure. The gold atom and blue atom are cobalt type I and II respectively. (b) Scattering pathways from cobalt type I atom in ε-Co (c) Scattering pathways from cobalt type II atom in ε-Co. Paths of the same length are represented with lines of the same color.

Table S1 The conditions of scattering pathways from cobalt type I atom in ε-Co

Numbers corresponding to Fig. S3 (b)	Pathway Distance(Å)	Number of Pathways	Scattering Atom
1	2.28	3	Co(I)
2	2.49	3	Co(II)
3	2.54	3	Co(II)
4	2.59	3	Co(II)

Table S2 The conditions of scattering pathways from cobalt type II atom in ε-Co

Numbers corresponding to Fig. S3 (c)	Pathway Distance(Å)	Number of Pathways	Scattering Atom
1	2.49	2	Co(I)
2	2.54	2	Co(I)
3	2.55	4	Co(II)
4	2.58	2	Co(II)
5	2.59	2	Co(I)

2) Co_2P

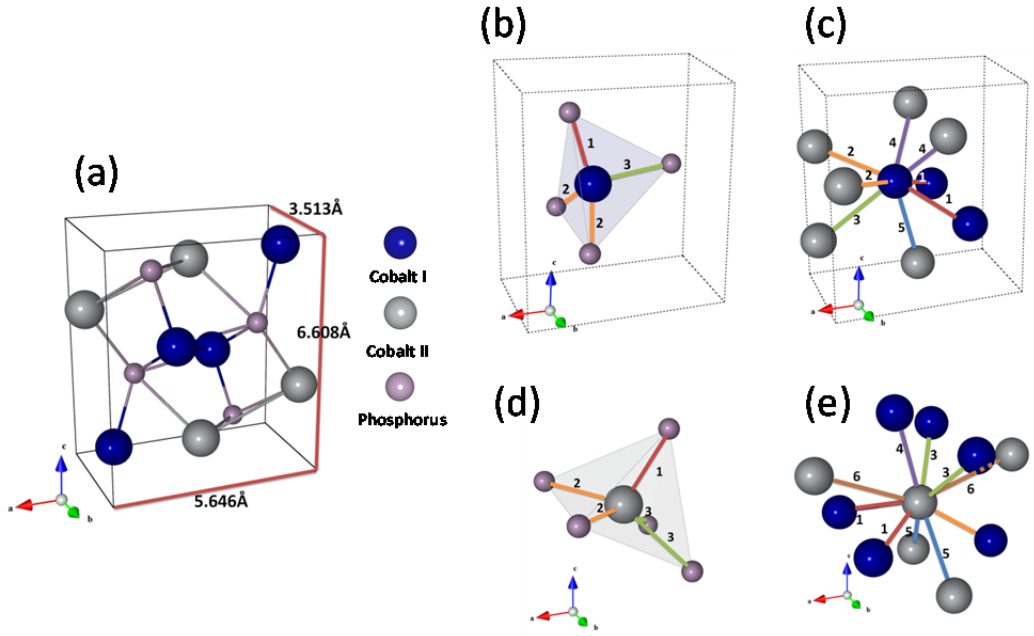

Fig S4 (a) A schematic representation of the Co_2P crystal structure. The blue, gray, and purple atoms are cobalt type I, II, and phosphorus respectively. (b) Co-P Scattering pathways from cobalt type I atom of Co_2P (c) Co-Co Scattering pathways from cobalt type I atom of Co_2P (d) Co-P Scattering pathways from cobalt type II atom of Co_2P (e) Co-Co Scattering pathways from cobalt type II atom of Co_2P.

Table S3 The conditions of Co-P scattering pathways from cobalt type I atom in Co_2P

Numbers corresponding to Fig. S4 (b)	Pathway Distance(Å)	Number of Pathways	Scattering Atom
1	2.14	1	P
2	2.23	2	P
3	2.24	1	P

Table S4 The conditions of Co-Co scattering pathways from cobalt type I atom in Co_2P

Numbers corresponding to Fig. S4 (c)	Pathway Distance(Å)	Number of Pathways	Scattering Atom
1	2.54	2	Co(I)
2	2.62	2	Co(II)
3	2.67	1	Co(II)
4	2.69	2	Co(II)
5	2.71	1	Co(II)

Table S5 The conditions of Co-P scattering pathways from cobalt type II atom in Co_2P

Numbers corresponding to Fig. S4 (d)	Pathway Distance(Å)	Number of Pathways	Scattering Atom
1	2.29	1	P
2	2.40	2	P
3	2.54	2	P

Table S6 The conditions of Co-Co scattering pathways from cobalt type II atom in Co_2P

Numbers corresponding to Fig. S4 (e)	Pathway Distance(Å)	Number of Pathways	Scattering Atom
1	2.62	2	Co(I)
2	2.67	1	Co(I)
3	2.69	2	Co(I)
4	2.71	1	Co(I)
5	2.83	2	Co(II)
6	3.03	2	Co(II)

2) CoP

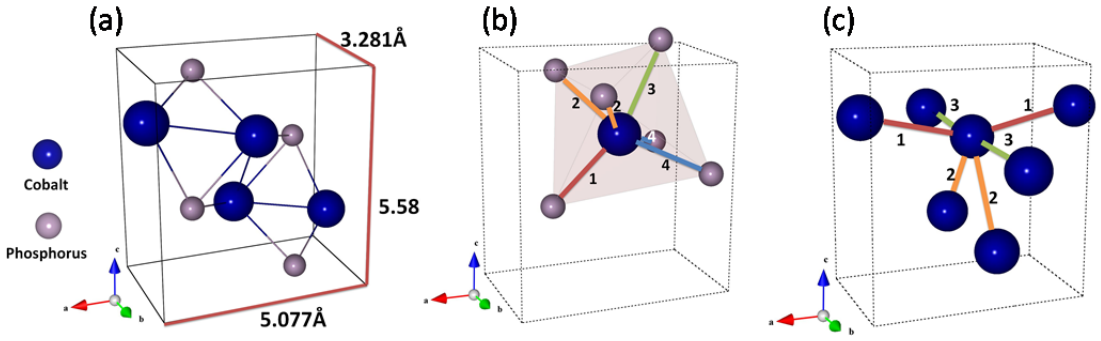

Fig. S5 (a) A schematic representation of the CoP crystal structure. The blue atom and purple atom are cobalt and phosphorus respectively. (b) Co-P Scattering pathways from cobalt atom in CoP (c) Co-Co Scattering pathways from cobalt atom in CoP.

Table S7 The conditions of Co-P scattering pathways from cobalt atom in CoP

Numbers corresponding to Fig. S5 (b)	Pathway Distance(Å)	Number of Pathways	Scattering Atom
1	2.21	1	P
2	2.27	2	P
3	2.35	1	P
4	2.36	2	P

Table S8 The conditions of Co-Co scattering pathways from cobalt atom in CoP

Numbers corresponding to Fig. S5 (c)	Pathway Distance(Å)	Number of Pathways	Scattering Atom
1	2.60	2	Co
2	2.76	2	Co
3	3.28	2	Co

Electronic Supplementary Material (ESI) for Journal of Materials Chemistry

EXAFS Analysis Methods

The raw absorption spectra obtained (Fig. S6) at the beamline were averaged and processed using the ATHENA software. This processing included edge determination from the first inflection point in the absorption data, background subtraction using the AUTOBK algorithm, and normalization of the EXAFS modulations (greater than 150 eV above the edge). A k-weight of 1 was chosen in order to emphasize the first coordination shell for fitting due to the presence of low-Z scatterers. The spectra were converted from E-space, to k-space, and then underwent a phase shift specific to the scattering element and Fourier transformation into R-space using the Hanning-type window, in order to better visualize the spacing and fit to theory. In a Fourier transform of the raw spectral data, each peak appears at the relative spacing of that particular shell from the scattering atom. The data, after processing, was then analyzed by the ab-initio method with use of the ARTEMIS software. Crystal structures from theory were inputted using ATOMS. By fitting well-matched theoretical pathways to the experimental spectra by loosening variables to deviate from the theoretical bulk structures, specific structural information was determined such as coordination number, spacing, and mean square disorder.

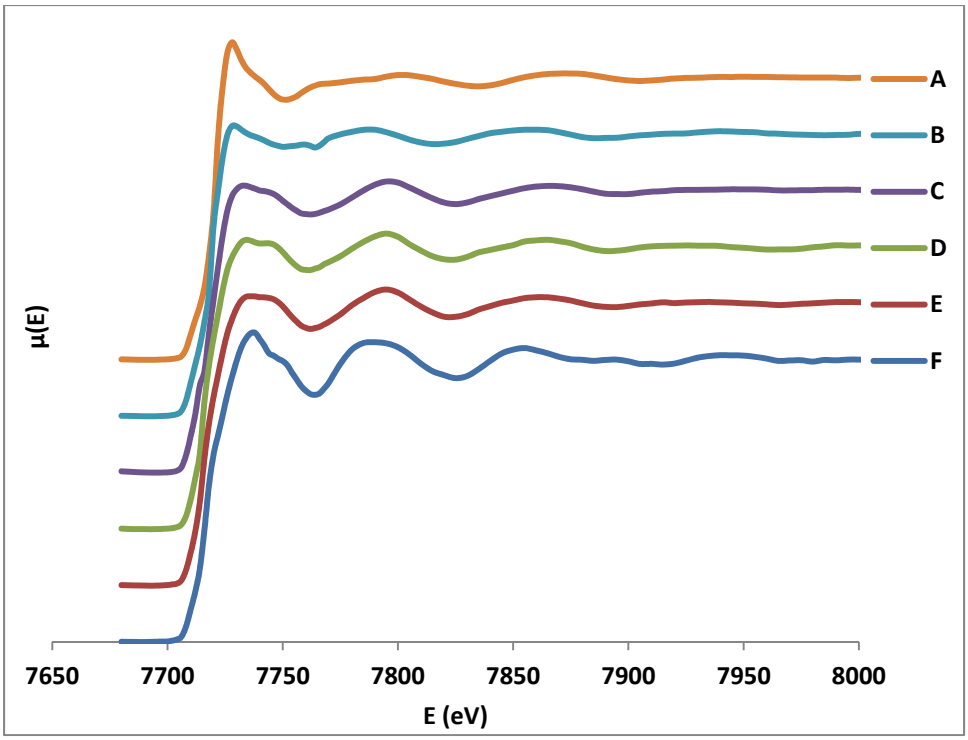

Fig. S6 Co K-edge XAS spectra: Samples **A** to **F**. The waterfall plot shows the absorption data obtained at the beamline. Even before analysis, a visual difference can be traced as the reaction progresses in the shape and definition of each spectrum.

EXAFS fitting details and procedure

The following EXAFS plots show the Fourier Transformations of the absorption spectrum obtained for each sample, their respective fitting using theoretical pathways, and residual pathway summations. The pathway summations shown were those used in the fitting process. Separate residuals represent a separate set of variables allowed to float during the fit.

1) Sample **A**

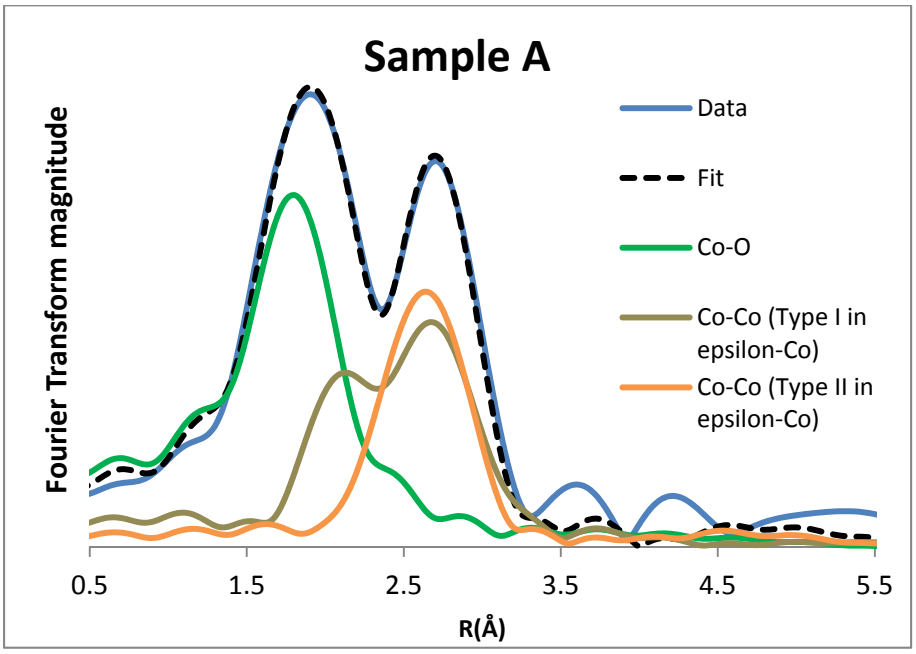

Fig. S7 The residual sums for sample **A** include the Co-O contribution at a short distance from the absorbing atom as well as Co-Co contributions using both type I and type II cobalt as the core.

Table S9 Sample **A** pathways and associated variable summary

Pathways	**Total Average Degeneracy**	**ΔE_0 (eV)**	**ΔR (Å)**	**σ^2**
Co_1 to Co_1	1.12	8.3098	-0.1387	0.015019
Co_1 to Co_2/ Co_2 to Co_1	7.728	9.999318	0.01906	0.017342
Co_2 to Co_2	2.23	-7.01082	0.04101	0.011824
Co to O	0.978	-8.739076	-0.229	0.0021

Table S10 Summary of fit parameters for Sample **A**.

	Values
Total Co-Co average coordination number	11.1
Total Co-O average coordination number	0.98
Reduced chi square value	288.68
R-factor	0.001410295
Path Used for Phase Shift	Co-Co

2) Sample **B**

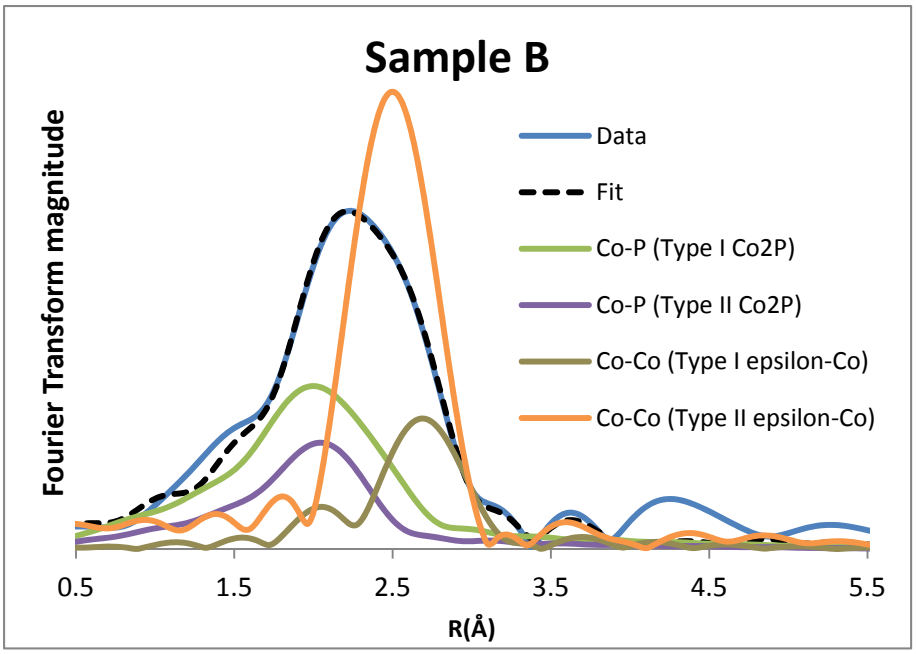

Fig. S8 The contributions to the Sample **B** spectrum include pathways from epsilon cobalt as well as a smaller amount of Co-P at a shorter bonding distance

Table S11 Sample **B** pathways and associated variable summary

Pathways	**Total Average Degeneracy**	**ΔE_0 (eV)**	**ΔR (Å)**	**σ^2**
Co_1 to Co	4.32	-4.659989	0.14266	0.00996
Co_2 to Co	5.88	6.902365	-0.023126	0.009057
Co_a to P	2.45	-8.955041	-0.16	0.007392
Co_b to P	0.96	-9.999989	0.020076	0.011527

Table S12 Summary of fit parameters for Sample **B**.

	Values
Total Co-Co average coordination number	10.2
Total Co-P average coordination number	3.41
Reduced chi square value	99.577537
R-factor	0.000874373
Path Used for Phase Shift	Co-Co

3) Sample **C**

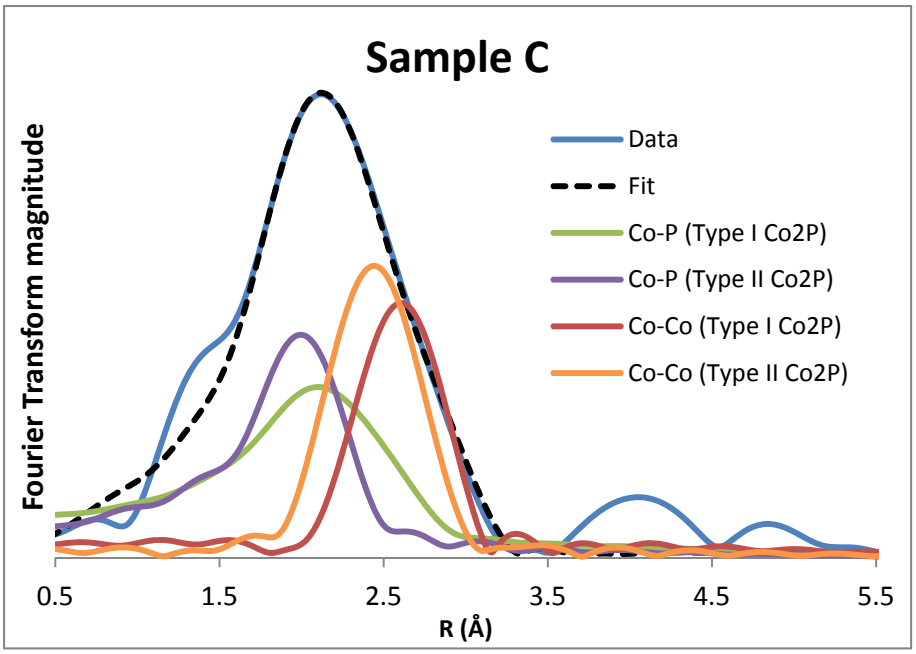

Fig. S9 The residual sums associated with sample **C** reveal the increased Co-P contribution due to increased Phosphorus diffusion

Table S13 Sample **C** pathways and associated variable summary

Pathways	**Total Average Degeneracy**	**ΔE_0 (eV)**	**ΔR (Å)**	**σ^2**
Co_A to P	3.325	-10	-0.152932	0.011932
Co_B to P	1.08	-7.471694	-0.069252	0.005759
Co_A to Co	7.3	-1.269713	-0.017524	0.012653
Co_B to Co	2.8548	-5.788145	-0.159	0.006055

Table S14 Summary of fit parameters for Sample **C**.

	Values
Total Co-Co average coordination number	10.2
Total Co-P average coordination number	4.4
Reduced chi square value	480.6568
R-factor	0.001654547
Path Used for Phase Shift	Co-Co

4) Sample **D**

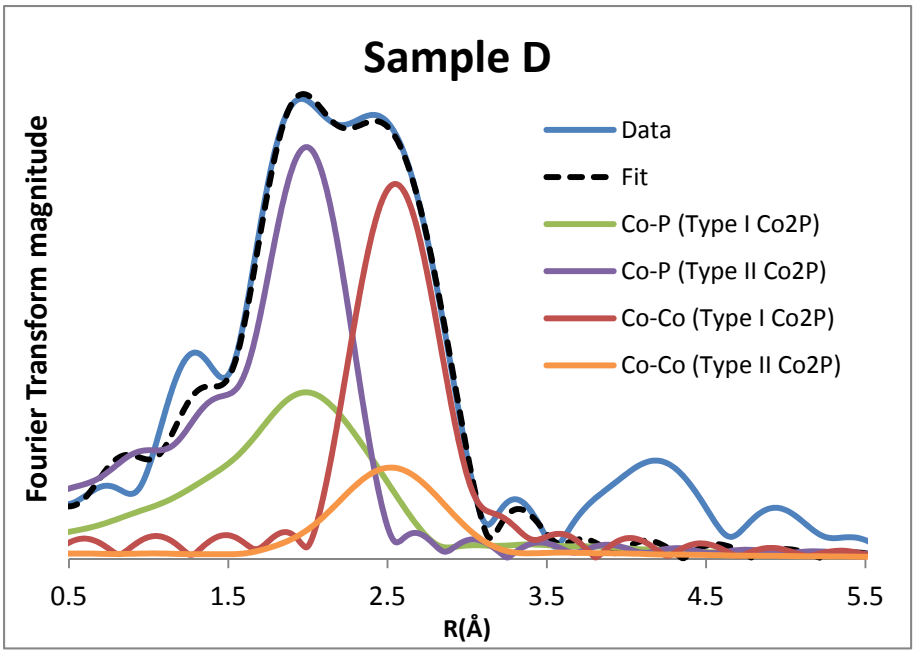

Fig. S10 The FT for sample **D** reveals two distinct peaks, associated with Co-P and Co-Co contributions. This reveals increased crystalline order within the structure, as the contributions become distinct.

Table S15 Sample **D** pathways and associated variable summary

Pathways	**Total Average Degeneracy**	**ΔE_0 (eV)**	**ΔR (Å)**	**σ^2**
Co_A to P	2.825	-10	-0.105952	0.010464
Co_B to P	1.84	-6.44098	-0.066952	0.002659
Co_A to Co	6.3	-1.545924	-0.075272	0.005416
Co_B to Co	3.58904	-4.121373	-0.025223	0.023724

Table S16 Summary of fit parameters for Sample **D**.

	Values
Total Co-Co average coordination number	9.9
Total Co-P average coordination number	4.7
Reduced chi square value	86.900344721
R-factor	0.000639151
Path Used for Phase Shift	Co-Co

5) Sample **E**

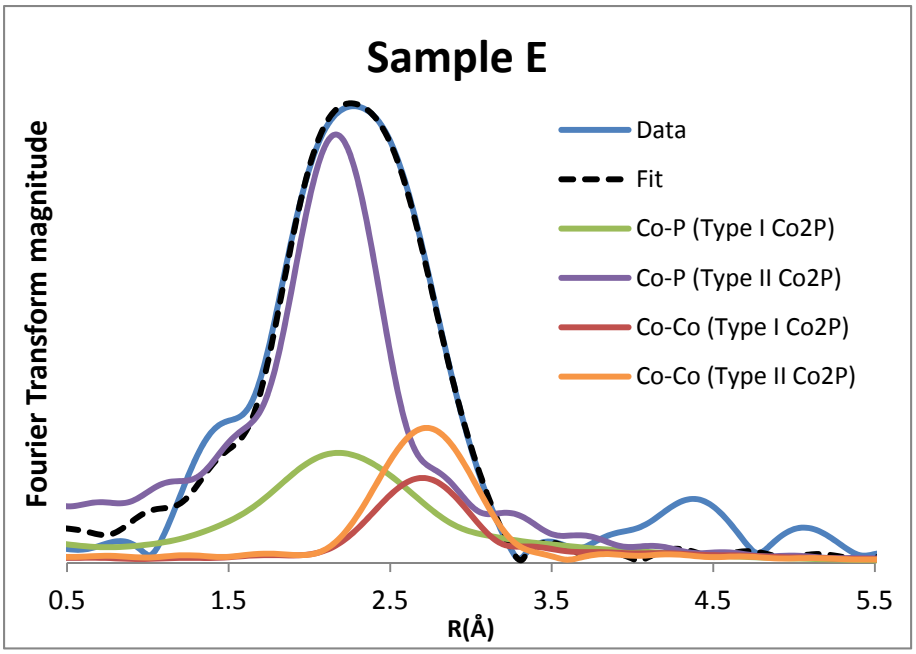

Fig. S11 The residual sums which contribute to sample **E** reveal a decrease in order, as the two distinct contributions are no longer distinguishable at separate distances as observed in sample **D**

Table S17 Sample **E** pathways and associated variable summary

Pathways	**Total Average Degeneracy**	**ΔE_0 (eV)**	**ΔR (Å)**	**σ^2**
Co_A to P	3.075	-10	-0.088822	0.017251
Co_B to P	2.84	-2.546812	-0.014710	0.006905
Co_A to Co	4.9	1.596878	-0.060017	0.02000
Co_B to Co	3.188984	-0.64398	0.0158	0.012375

Table S18 Summary of fit parameters for Sample **E**.

	Values
Total Co-Co average coordination number	8.1
Total Co-P average coordination number	5.9
Reduced chi square value	86.900344721
R-factor	0.000639151
Path Used for Phase Shift	Co-P

6) Sample **F**

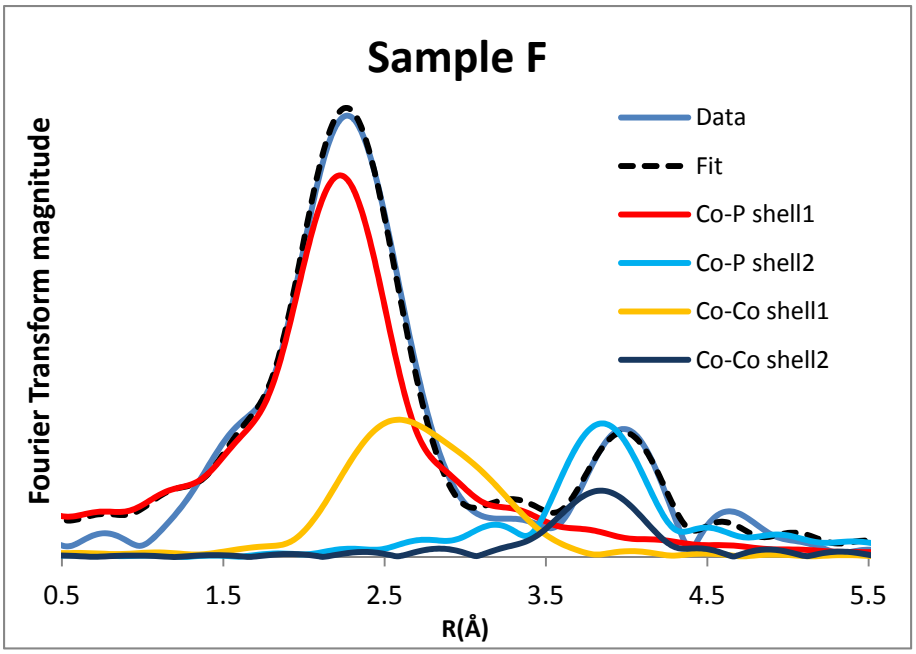

Fig. S12 The FT for sample **F** shows an apparent second shell contribution, associated with long-range order with increased crystallinity.

Table S19 Sample **F** pathways and associated variable summary

Pathways	**Total Average Degeneracy**	**ΔE_0 (eV)**	**ΔR (Å)**	**σ^2**
Co to P shell 1	5.52	-3.032113	-0.036685	0.008577
Co to Co shell 1	7.524	-6.497283	-0.132	0.010045
Co to P shell 2	8.48	5.084003	-0.061169	0.003803
Co to Co shell 2	2.46	1.452831	0.049239	0.002997

Table S20 Summary of fit parameters for Sample **F**.

	Values
Total Co-Co average coordination number	7.5
Total Co-P average coordination number	5.5
Reduced chi square value	355.397899926
R-factor	0.008133337
Path Used for Phase Shift	Co-P

Calculation of the concentration of atoms on the surface in a nanoparticle

The average nanoparticle size was estimated by TEM. Spherical Cluster Approximation (SCA) was used in this calculation.[1] We assumed that the NPs are spherical.

$$V_{cluster} \approx NV_{atom} \quad (1)$$

$$\frac{4}{3}\pi(R_{cluster})^3 = N\frac{4}{3}\pi(R_{atom})^3 \quad (2)$$

Where N is the total number of atoms in the cluster, V is cluster/atom volume, and R is radius of cluster/atom. After rearranging, we obtain:

$$R_{cluster} = N^{1/3}R_{atom} \quad (3)$$

By using $R_{cluster}$ as 5.95nm which was obtained by TEM analysis and R_{cobalt} as 0.135nm, the number of atoms in NP is 85615.

$$S_{cluster} = 4\pi R_{cluster}^2 \quad (4)$$

S is the surface area of cluster/atom. The number of surface atoms N_s in a cluster is given by dividing the surface area of the cluster by the cross-sectional area of an atom (A_a). After rearranging, we obtain:

$$N_s = \frac{4\pi(R_{cluster})^2}{\pi R_{atom}^2} = 4N^{2/3} \quad (5)$$

From this equation, the number of surface atoms is 7770. Therefore, the fraction of the surface atoms is about 9%. (≈ 7770/85615)

Calculation Details

Total energy calculations were carried out using the Vienna Ab-initio Software Package (VASP),[2-5] within the framework of DFT. The gradient- corrected PBE exchange-correlation functional was employed,[6] along with the Projector Augmented Wave (PAW) method.[7, 8] For density of state calculations the hybrid HSE06 functional was also employed.[9] Calculations were carried out with periodic boundary conditions, with wave functions expanded on a plane-wave basis set. K-sampling of the Brillouin zone was performed using special k-points generated using the method of Monkhorst and Pack.[10] For density of states (DOS) calculations in which the PBE functional was employed, K-point meshes of 12×12×12 and 13×21×11 were employed, for the ε-Co and Co_2P/ CoP cells, respectively. For DOS calculations in which the HSE06 functional was employed, K- point meshes of 6×6×6 and 8×12×6 were employed, for the ε-Co and Co_2P/CoP cells, respectively. The kinetic energy cutoff for the wave functions was set to 351.0 eV for DOS calculations in which the PBE functional was employed, and 270.0 eV for DOS calculations in which the HSE06 functional was employed. The corresponding cutoff energies for the augmentation functions were set to 621.2 eV and 477.8 eV. For nudged elastic band (NEB) calculations, the same k-point meshes and cutoff energies were used as for the HSE06 DOS calculations. The corresponding cutoff energies for the augmentation functions were set to 621.2 eV and 477.8 eV.

Density of States for Co_2P and CoP

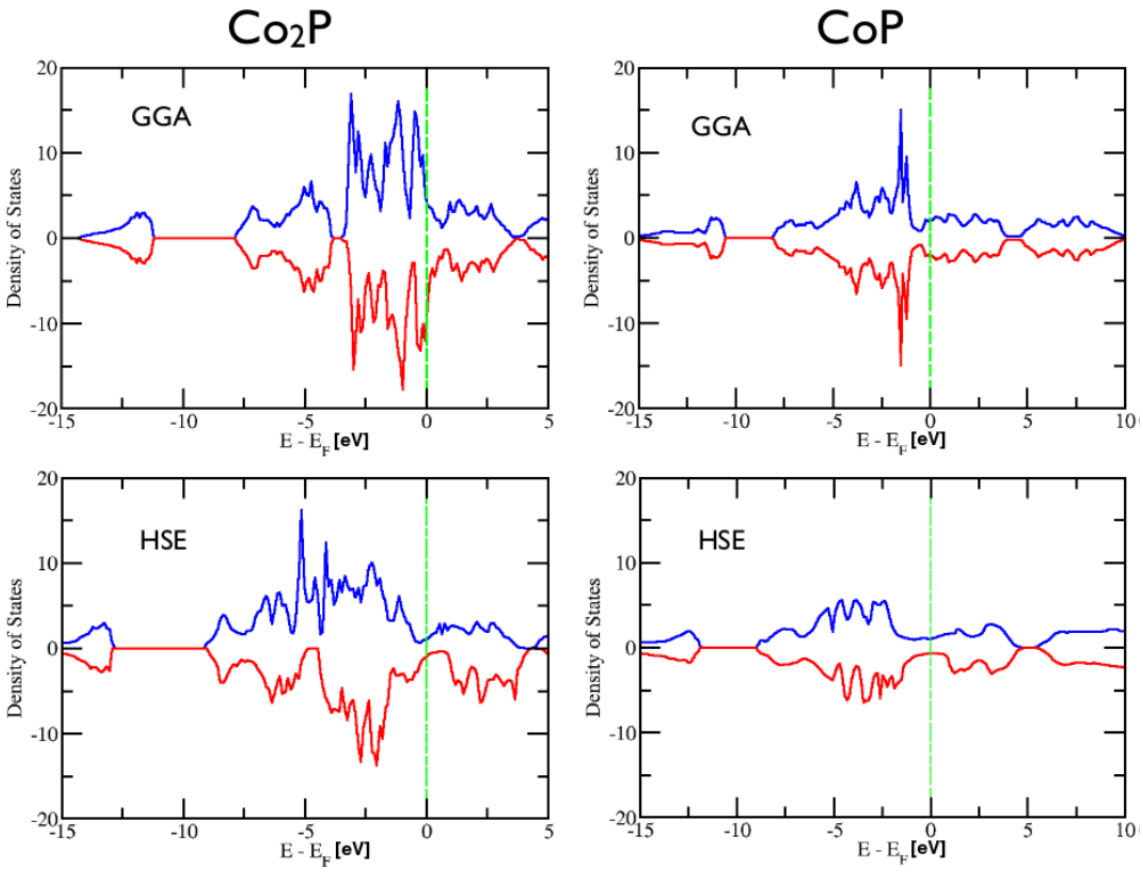

Fig. S13 Total DOS plots for the Co_2P and CoP structures for the GGA PBE exchange-correlation functional and HSE06 hybrid functional. Spin up (blue lines) and spin down (red lines) contributions are represented in each case.

1. R. L. Johnston, *Atomic and Molecular Clusters*, Taylor & Francis, 2002.
2. G. Kresse and J. Hafner, *Phys. Rev. B*, 1993, **47**, 558.
3. G. Kresse and J. Hafner, *Phys. Rev. B*, 1994, **49**, 14251.
4. G. Kresse and J. Furthmüller, *Comput. Mater. Sci.*, 1996, **6**, 15-50.
5. G. Kresse and J. Furthmüller, *Phys. Rev. B*, 1996, **54**, 11169.
6. J. P. Perdew, K. Burke and M. Ernzerhof, *Phys. Rev. Lett.*, 1996, **77**, 3865.
7. P. E. Blöchl, *Phys. Rev. B*, 1994, **50**, 17953.
8. G. Kresse and D. Joubert, *Phys. Rev. B*, 1999, **59**, 1758.
9. J. Paier, M. Marsman, K. Hummer, G. Kresse, I. C. Gerber and J. G. Angyan, *The Journal of Chemical Physics*, 2006, **124**, 154709-154713.
10. H. J. Monkhorst and J. D. Pack, *Phys. Rev. B*, 1976, **13**, 5188.